Investigation on porosity and permeability change of Mount Simon sandstone

(Knox County, IN) under geological CO<sub>2</sub> sequestration conditions: a

numerical simulation approach

Liwei Zhang\*, Yee Soong and Robert M. Dilmore

U.S. Department of Energy, National Energy Technology Laboratory, 626 Cochrans Mill Road, P.O. Box

10940, Pittsburgh, PA 15236

\* Corresponding author

Phone: +1-412-386-5364

E-mail address: liwei.zhang@netl.doe.gov

Abstract

A numerical model was developed to simulate reactive transport with porosity and permeability

change of Mount Simon sandstone (samples from Knox County, IN) after 180 days of exposure

to CO<sub>2</sub>-saturated brine under CO<sub>2</sub> sequestration conditions. The model predicted formation of a

high-porosity zone adjacent to the surface of the sample in contact with bulk brine, and a lower

porosity zone just beyond that high-porosity zone along the path from sample/bulk brine

interface to sample core. The formation of the high porosity zone was attributed to dissolution of

quartz and muscovite/illite, while the formation of the lower porosity zone adjacent to the

aforementioned high porosity zone was attributed to precipitation of kaolinite and feldspar. The

model predicted a 40% permeability increase for the Knox sandstone sample after 180 days of

exposure to CO<sub>2</sub>-saturated brine, which was consistent with laboratory-measured permeability

results. Model-predicted solution chemistry results were also found to be consistent with

laboratory-measured solution chemistry data. Initial porosity, initial feldspar content and the

exponent n value (determined by pore structure and tortuosity) used in permeability calculations

were three important factors affecting permeability evolution of sandstone samples under CO<sub>2</sub>

sequestration conditions.

1

# **Key words**

CO<sub>2</sub> sequestration; reactive transport; porosity; permeability; sandstone

## Introduction

Carbon capture and storage (CCS) is a promising strategy to reduce the emissions of carbon dioxide (CO<sub>2</sub>) to the atmosphere <sup>1-3</sup>. Coal seams, depleted oil reservoirs and saline aquifers are three CO<sub>2</sub> storage targets that offer opportunity for underground storage of significant quantity of  $CO_2^{1,4}$ . Among the three  $CO_2$  storage pathways, saline aquifers have the highest estimated CO<sub>2</sub> storage capacity — at least 1,738 Gigatonnes of CO<sub>2</sub> in North America alone<sup>5</sup>. Mount Simon Sandstone formation in the Illinois Basin (Illinois and Indiana) is one of the target saline aquifers for large quantity CO<sub>2</sub> storage, because the Mount Simon formation has thick net interval with fair to good permeability and porosity, and the overlying strata contain impermeable limestone, dolomite, and shale intervals<sup>6</sup>. To study how Mount Simon sandstone samples react with injected CO<sub>2</sub>, Soong et al. exposed samples taken from both Vermillion County, IN and Knox County, IN to CO<sub>2</sub>-saturated brine under laboratory-simulated CO<sub>2</sub> storage conditions  $(P = 23.8 \text{ MPa} \text{ and } T = 85 \text{ }^{\circ}\text{C})^{7}$ . They observed a 50% permeability decrease after 180 days of exposure for sandstone samples taken from Vermillion County, while they observed a 38% permeability increase after 180 days of exposure for sandstone samples taken from Knox County (hereafter referred to as Knox samples)<sup>7</sup>.

To probe the question of what mineral precipitation/dissolution processes cause porosity and permeability changes of Vermillion and Knox samples, a numerical model is developed using

reactive transport code CrunchFlow<sup>8</sup> to simulate the mineral precipitation/dissolution processes of Vermillion and Knox samples exposed to CO<sub>2</sub>-saturated brine. Model-predicted permeability change of Vermillion sandstone after 180 days of exposure has been presented in Zhang et al., (2015)<sup>8</sup>. This paper presents permeability change of Knox samples and explains why Vermillion samples and Knox samples have different permeability evolution patterns during the 180-day exposure period.

Numerical simulations of mineral dissolution and precipitation in the context of CO<sub>2</sub> storage have been presented in many papers<sup>8-14</sup>. This study is based on previous efforts in mineral dissolution and precipitation modeling, and a porosity/permeability model is coupled with the mineral dissolution and precipitation model to predict how mineral dissolution and precipitation affect porosity and permeability of Knox sandstone samples.

## Methodology

A 1-D reactive transport model was developed using simulation code CrunchFlow<sup>15-16</sup>. Key assumptions of CrunchFlow and important governing equations used in CrunchFlow are provided in the Supporting Information section. A schematic of the modeled region is provided in Figure 1. The brine domain was divided into 100 grid blocks, with each block assigned a length of 1.48 mm; the sandstone domain was divided into 1,000 grid blocks, with each block assigned a length of 0.0254 mm. The initial rock: water volumetric ratio was taken to be the same as the volumetric ratio of brine to the Knox sample in the reactor for experiments by Soong et al.<sup>7</sup>. The model simulates the following processes: 1) dissolution of minerals that are initially present in Knox sandstone due to penetration of [H<sup>+</sup>] and dissolved CO<sub>2</sub> into the sandstone under

CO<sub>2</sub> sequestration conditions; 2) release of ions into the pore space of Knox sandstone from dissolution of minerals; 3) reactions of released ions with CO<sub>2</sub> and other ions to form minerals that may precipitate in the pore space. Minerals involved in the simulation and their specific surface area and molar volume can be found in Table 1, and equilibrium constant and reaction rate constant for each mineral can be found in Zhang et al. 8. As suggested in Carroll et al. (2012)<sup>13</sup>, three secondary minerals (montmorillinite, kaolinite and SiO<sub>2</sub> (am)) were included in the model. Siderite, gypsum, barite, calcite and dolomite were also included in the model due to their potential to precipitate under the modeling scenario. All specific surface areas, molar volumes, equilibrium constants and reaction rate constants were obtained from literature search. Initial brine composition used in the model can be found in Table 2. The porosity of the unreacted Knox sample was 1.4%, and the permeability of the unreacted Knox sample was 50 nD. The porosity of the unreacted sample was measured using a helium porosimeter (HP-41, Temco, Inc) at 0.7 MPa and ambient temperature, and the permeability of the unreacted sample was measured using an Autolab 1500 unit (New England Research, Inc.). The maximum simulation time was 180 days. The modeled system is a closed system with no flow, so as to mimic the experimental conditions employed in Soong et al.<sup>7</sup>. Details of the experimental design and experimental conditions can be found in Soong et al. 7. Important governing equations used in the model can be found in the Supporting Information section.

The model used in this study is a no flow 1-D model, which has limitations. Firstly, the no-flow system used in this study considers only diffusive transport of aqueous species, while a flow-through system allows advective transport of aqueous species, which sometimes accelerates dissolution and precipitation of minerals. Secondly, the model cannot model formation of

preferential flow pathways (wormholes) or expansion of existing wormholes. Previous studies do show that flowing CO<sub>2</sub>-saturated brine through sandstone may cause formation or expansion of wormholes in sandstone, and the degree of wormhole formation/expansion depends on mineral compositions of sandstone, size of pre-existing wormhole and flow rate<sup>17-18</sup>.

Porosity and permeability results obtained from Knox samples were compared with results from samples taken from Vermillion County, IN, which have been published in Zhang et al. (2015)<sup>8</sup>. Both samples are sandstone samples taken from Mount Simon formation and are rich in quartz and feldspar. Compared with unreacted Knox samples, unreacted Vermillion samples contain higher quartz content (77.0 vol% quartz *v.s.* 69.8 vol% quartz in Knox samples) and lower total feldspar content (15.0 vol% total feldspar *v.s.* 22.0 vol% total feldspar in Knox samples). Unreacted Vermillion samples contain no muscovite/illite, while unreacted Knox samples contain 4 vol% muscovite/illite. Unreacted Vermillion samples have a much higher porosity (7.9%) than that of unreacted Knox samples (1.4%).

## **Results and discussion**

Solution chemistry, porosity and mineral composition results

Table 2 shows a comparison between model-predicted major element concentrations in brine after 180 days of exposure and laboratory-measured major element concentrations after 180 days of exposure. The concentrations predicted by the model were consistent with measured concentrations. For Ca, Na, Mg and K, the difference between model-predicted concentrations and measured concentrations was less than 5%. The model-predicted concentrations of Na and K were slightly lower than those measured in the experiment, which implies that the model slightly

under-predicts the dissolution rate of muscovite/illite, and over-predicts the precipitation rate of feldspar. For Fe and Si, the model-predicted concentrations were higher than those measured in the experiment (145 mg/kg water v.s. 91.9 mg/kg water for Fe and 17.8 mg/kg water v.s. 10.0 mg/kg water for Si). Many complexation reactions are associated with Fe and Si-bearing species in solution and there is a large standard deviation between measured Si concentration values, which may contribute to the difference between model-predicted Fe and Si concentrations and measured concentrations. For Al and Ba, the model-predicted concentrations were lower than those measured in the experiment (0.26 mg/kg water v.s.1.42 mg/kg water for Al and 0.13 mg/kg water v.s.2.95 mg/kg water for Ba). The lower an element concentration is, the harder for the model to fit experimental data, because a slight deviation of model parameters from real values will cause significant change in model-predicted element concentration. The concentration of dissolved inorganic carbon in brine (8,268 mg/kg water, which equals to 0.689 mol/kg water) was the same as the starting concentration after 180 days of exposure, which implies minimal formation of calcite and dolomite in Knox samples during the 180-day simulation time.

Figure 2 shows porosity change from the surface of Knox samples in contact with bulk brine to the interior of the samples at varying exposure times, and Figure 3 (a ~ g) shows volume fraction changes of key minerals. Two distinct zones in Figure 2 are defined below: Zone 1—sandstone/brine interface to deepest point of dissolution (mineral dissolution zone); Zone 2—deepest point of dissolution to the interior of the sample (mineral precipitation zone). A fast increase in porosity in Zone 1 with the increase of exposure time is predicted as illustrated in Figure 2. The fast increase in porosity was mainly attributed to dissolution of quartz (Figure 3d) and muscovite/illite (Figure 3f). Dissolution of quartz and illite in sandstone when exposed to

CO<sub>2</sub>-rich brine has been reported by previous studies<sup>13, 19</sup>. In Zone 2, there was a porosity decrease from day 0 to 180 days of exposure to CO<sub>2</sub>-saturated brine. The porosity decrease was mainly caused by precipitation of feldspar (Figure 3a) and kaolinite (Figure 3g). Precipitation of feldspar is not commonly reported under typical CO<sub>2</sub> storage conditions, but our modeling work shows that dissolution of muscovite/illite can provide Al source for feldspar precipitation given a short exposure period (e.g., 180 days). Precipitation of kaolinite is commonly reported in CO<sub>2</sub>-exposure experiments and numerical simulation studies<sup>8, 20-21</sup>.

# Permeability results

Porosity results obtained from the 1-D model show that there is a high-porosity zone (Zone 1) adjacent to the sandstone surface after 180 days of exposure to CO<sub>2</sub>-saturated brine, and the zone next to the high-porosity zone (Zone 2) exhibits low porosity and low permeability (Figure 4). Because the vertical permeability (along the flow direction of the cylindrical sample, see Figure 4) of the entire sample is governed by the zone with the lowest permeability, the permeability in vertical direction of the sandstone is approximately equal to the permeability of a third composite zone (Zone 3, composed of grid cells from Zone 1 at the edges and grid cells from Zone 2 at the center, see Figure 4). The permeability of Zone 3 can be calculated as<sup>22</sup>:

$$perm_{v,t} = \frac{\sum_{i=1}^{n} l_{i} perm_{i,t}}{L}$$
 (1)

where  $perm_{v,t}$  is the vertical permeability of Zone 3 at time t; L is the width of Zone 3 (2.54 cm);  $l_i$  is the size of the individual block (2.54 × 10<sup>-3</sup> cm);  $perm_{i,t}$  is the local permeability of the grid block i at time t, and n is the total number of cells (1,000).

The correlation between  $perm_{i,t}$  and grid block porosity at time t can be written as<sup>23</sup>:

$$\frac{perm_{i,t}}{perm_{i,0}} = (\frac{\emptyset_{i,t}}{\emptyset_{i,0}})^n \tag{2}$$

where  $perm_{i,t}$  is the local permeability of the grid block i at time t;  $perm_{i,0}$  is the initial permeability of the grid block i (for all grid blocks,  $perm_{i,0}$  is equal to 50 nD);  $\phi_{i,t}$  is the porosity of the grid block i at time t;  $\phi_{i,0}$  is the initial porosity of the grid block i (for all grid blocks,  $\phi_{i,0}$  is equal to 0.014). n is an exponential coefficient, which is set to be 4.9 (this value lies in the range of 3 to 75 for different types of cement and rock materials reported by Brunet et al.<sup>23</sup>). An n value of 4.9 produces simulation results that are closest to laboratory-measured permeability result (see Table S-1 in Supporting Information for details).

Figure 5-a shows porosity distribution at Zone 3, and Figure 5-b shows the permeability of Zone 3 calculated from porosity distribution in Figure 5-a. The porosity in the high-porosity zone was much higher than initial porosity (max. 5.0% vs. 1.4%), and the lowest porosity in the low-porosity zone was 24% lower than the initial porosity. Due to the existence of the high-porosity zone, the calculated permeability of Zone 3 was higher than the initial permeability (70.5 nD vs. 50.0 nD). That is to say, the model predicts a 41% permeability increase of the Knox sandstone after 180 days of exposure to CO<sub>2</sub>-saturated brine. This result is very close to the laboratory-measured permeability result, which shows a 38% permeability increase after exposure <sup>7</sup>.

## Sensitivity analysis

Figure 6 shows how the initial porosity and initial feldspar content change affects permeability change after 180 days of exposure. A general trend is: sandstone with low initial porosity (i.e.,

1.4%) shows significant permeability increase (much higher than 50 nD) after 180 days of exposure; sandstone with moderate initial porosity (2.5 to 4%) shows permeability decrease (lower than 50 nD) after 180 days of exposure; sandstone with relatively high initial porosity (6 to 8%) shows very small permeability change after 180 days of exposure. An explanation to those results is: the relative porosity change in Zone 1 of the sample with low initial porosity is much larger than that of the sample with high initial porosity. For example, when the initial porosity equals 1.40% and initial feldspar content equals 5.80%, the highest porosity in Zone 1 is 5.45% after 180 days of exposure, which is about 4 times the initial porosity. Based on the permeability change equation  $\frac{p_{erm}}{p_{erm_{ini}}} = (\frac{p_{orosity}}{p_{orosity_{ini}}})^{4.9}$ , a porosity increase from 1.40% to 5.45% results in 780 times higher permeability than the initial permeability. When the initial porosity is 8.00% and initial feldspar content is 5.80%, the highest porosity in Zone 1 is 10.8% after 180 days of exposure, and a porosity increase from 8.00% to 10.8% only results in 3.4 times higher permeability than the initial permeability. Because the permeability increase in Zone 1 of the sample with 1.4% initial porosity is so large, net permeability increase is observed. However, for samples with moderate initial porosity (i.e., 2.5% to 4.0%), the permeability increase in Zone 1 is not big enough to offset permeability decrease in Zone 2, and net permeability decrease is observed. For samples with relatively high initial porosity (i.e., 6.0% to 8.0%), there is sufficient pore space and the precipitation of minerals does not significantly reduce the pore space available for flow migration. Therefore, the permeability change of samples with relatively high initial porosity is small. The small permeability change given high initial porosity is consistent with permeability results reported by Rimmelé et al.<sup>24</sup>, which shows minimal permeability change of sandstone samples with an initial porosity of 20% after exposure to CO<sub>2</sub>-saturated water for one month.

When initial porosity is low (i.e., 1.4% to 2.5%), increasing initial feldspar content (bulk vol%) results in a decrease in permeability after exposure. A brief explanation is: kaolinite precipitation follows both illite dissolution and feldspar dissolution. An increase in feldspar content results in more precipitation of kaolinite in Zone 2, which leads to lower permeability after exposure. When initial porosity is relatively high (i.e., 6.0% to 8.0%), increasing initial feldspar content results in an increase in permeability after exposure. A brief explanation is: more feldspar in Zone 1 gets dissolved after exposure to CO<sub>2</sub> given a higher initial feldspar content and the relative increase in permeability of Zone 1 becomes higher, which leads to overall permeability increase after exposure.

Comparison between results of Knox samples and results of Vermillion samples

Compared with the results of reacted Vermillion samples, the low-porosity zone of the reacted

Knox samples extended to the interior of the samples, and there was a significant precipitation of

feldspar in Knox samples, which was not observed in Vermillion samples (Figure 7). An

explanation to the different results is that, unreacted Knox County sandstone samples contain 4

vol% muscovite/illite, which dissolves readily under acidic conditions and provides Al source for

feldspar and kaolinite precipitation. Unreacted Vermillion County sandstone samples contain no

detectable muscovite/illite, which makes feldspar the Al source for kaolinite precipitation.

After 180 days of exposure, the permeability of the Knox sample increased by 41%, while the permeability of the Vermillion sample dropped by 36% (Figure 7). The very different results are primarily attributed to 1) different initial porosity and 2) different *n* value in Eqn 2. As discussed in the sensitivity analysis section, a sample with very low initial porosity like the Knox sample

tends to have a significant permeability increase after 180 days of exposure. The n value of the Knox sample (n = 4.9) is different from the n value of the Vermillion sample (n = 11) <sup>10</sup>, and a combination of higher initial porosity and higher n value for the Vermillion sample results in a permeability drop after 180 days of exposure. Given the fact that the exponent n is dependent on pore structure and tortuosity of the rock, our modeling results suggest that sandstone samples taken from Vermillion County, IN and Knox County, IN differ in pore structure and/or tortuosity, which results in different permeability evolution patterns. Core imaging techniques such as CT scanning could be used as an experimental basis to verify the aforementioned structural difference in future studies.

# Summary and Implications

Results from this study suggest that initial porosity, initial feldspar content and the exponent *n* (determined by pore structure and tortuosity) used in permeability calculations are three important factors that affect permeability evolution of sandstone samples exposed to CO<sub>2</sub> sequestration conditions. The permeability results obtained in this paper can be extended to other sandstone samples with similar mineral compositions and pore structure. Specifically, for sandstone samples with initial porosity between 2.5% and 4.0% and initial feldspar content between 5.80% and 21.0%, a permeability decrease after several months of exposure is expected. The permeability decrease suggests an enhanced containment of injected CO<sub>2</sub> in the storage formation, which is desired from the perspective of CO<sub>2</sub>plume stabilization and physical trapping of CO<sub>2</sub>. However, for samples with low initial porosity (i.e., 1.40%) and initial feldspar content between 5.80% and 21.0%, there is a possibility that permeability could increase after several months of exposure to CO<sub>2</sub>. However, because the initial permeability is low for those

samples (on the order of nD) and the formation that contains such low-permeability sandstone is probably not suitable for large-scale CO<sub>2</sub> storage, this observed phenomenon is not expected to be impactful to storage formation behavior or CO<sub>2</sub> leakage risk.

# **Supporting Information**

Supporting Information contains important governing equations used in the reactive transport model, and a table showing the reason to choose an exponent value (n) of 4.9 in Equation 2.

# Acknowledgments

This research was supported in part by an appointment to the National Energy Technology

Laboratory Research Participation Program, sponsored by the U.S. Department of Energy and
administered by the Oak Ridge Institute for Science and Education (ORISE). The authors would
like to thank the Office of Research and Development at NETL and ORISE for funding support
and providing access to research article databases, computing devices, etc. The authors also
would like to thank Bret Howard at NETL Pittsburgh site for valued suggestions on sample
characterization and result interpretation.

#### References

(1) White, C. M.; Strazisar, B. R.; Granite, E. J.; Hoffman, J. S. & Pennline, H. W. Separation and capture of CO<sub>2</sub> from large stationary sources and sequestration in geological formations—coalbeds and deep saline aquifers. *J. Air Waste Ma.*, **2003**, 53(6), 645-715. DOI: 10.1080/10473289.2003.10466206.

- (2) Gasda, S. E.; Nordbotten, J. M. and Celia, M. A. Determining effective wellbore permeability from a field pressure test: a numerical analysis of detection limits. *Environ. Geol.*, **2008**, 54, 1207–1215. DOI: 10.1007/s00254-007-0903-7.
- (3) Yang, Y. M.; Small, M. J.; Ogretim, E. O.; Gray, D. D.; Bromhal, G. S.; Strazisar, B. R. & Wells, A. W. Probabilistic design of a near-surface CO2 leak detection system. *Environ. Sci. Technol.*, **2011**, 45(15), 6380-6387. DOI: 10.1021/es104379m.
- (4) U.S. Department of Energy, Office of Fossil Energy, National Energy Technology Laboratory. Carbon Utilization and Storage Atlas. Morgantown, WV, USA, **2012**.
- (5) The North American Carbon Storage Atlas (NACSA). NACSA 2012 (1st Edition). Available at: http://www.netl.doe.gov/File%20Library/Research/Carbon-Storage/NACSA2012.pdf, **2012**.
- (6) Midwest Geological Sequestration Consortium. The science of sequestration. Available at: http://www.sequestration.org/science/index.html, **2014**.
- (7) Soong, Y.; Howard, B. H.; Hedges, S. W.; Haljasmaa, I.; Warzinski, R. P.; Irdi, G., & McLendon, T. R. CO<sub>2</sub> Sequestration in Saline Formation. *Aerosol Air Qual. Res.*, **2014**, 14(2), 522-532. DOI: 10.4209/aaqr.2013.06.0195.
- (8) Zhang, L.; Soong, Y.; Dilmore, R. and Lopano, C. Numerical simulation of porosity and permeability evolution of Mount Simon sandstone under geological carbon sequestration conditions. *Chemical Geology*, **2015**, 403, 1-12. DOI: 10.1016/j.chemgeo.2015.03.014.
- (9) Johnson, J. W., Nitao, J. J., & Knauss, K. G. (2004). Reactive transport modeling of CO<sub>2</sub> storage in saline aquifers to elucidate fundamental processes, trapping mechanisms and sequestration partitioning. *Geological storage of carbon dioxide*, 233, 107-128.
- (10) Xu, T., Apps, J. A., & Pruess, K. (2004). Numerical simulation of CO<sub>2</sub> disposal by mineral trapping in deep aquifers. *Applied geochemistry*, 19(6), 917-936.
- (11) Knauss, K. G., Johnson, J. W., & Steefel, C. I. (2005). Evaluation of the impact of CO<sub>2</sub>, co-contaminant gas, aqueous fluid and reservoir rock interactions on the geologic sequestration of CO<sub>2</sub>. *Chemical Geology*, 217(3), 339-350.
- (12) Beyer, C., Li, D., De Lucia, M., Kühn, M., & Bauer, S. (2012). Modelling CO<sub>2</sub>-induced fluid–rock interactions in the Altensalzwedel gas reservoir. Part II: coupled reactive transport simulation. *Environmental Earth Sciences*, 67(2), 573-588.
- (13) Carroll, S. A., McNab, W. W., Dai, Z., & Torres, S. C. (2012). Reactivity of Mount Simon sandstone and the Eau Claire shale under CO<sub>2</sub> storage conditions. *Environmental Science & Technology*, 47(1), 252-261.

- (14) Klein, E., De Lucia, M., Kempka, T., & Kühn, M. (2013). Evaluation of long-term mineral trapping at the Ketzin pilot site for CO<sub>2</sub> storage: an integrative approach using geochemical modelling and reservoir simulation. *International Journal of Greenhouse Gas Control*, 19, 720-730.
- (15) Steefel, C. I. CrunchFlow User's Manual. Lawrence Berkeley National Laboratory: Berkeley, CA, **2009**.
- (16) Steefel, C. I., & Maher, K. (2009). Fluid-rock interaction: A reactive transport approach. *Reviews in mineralogy and geochemistry*, 70(1), 485-532.
- (17) Smith, M. M., Sholokhova, Y., Hao, Y., & Carroll, S. A. (2012). Evaporite caprock integrity: An experimental study of reactive mineralogy and pore-scale heterogeneity during brine-CO<sub>2</sub> exposure. *Environmental Science & Technology*, 47(1), 262-268.
- (18) Ott, H., & Oedai, S. (2015). Wormhole formation and compact dissolution in single-and two-phase CO<sub>2</sub>-brine injections. *Geophysical Research Letters*, 42(7), 2270-2276.
- (19) Carroll, S. A., McNab, W. W., & Torres, S. C. (2011). Experimental study of cement-sandstone/shale-brine-CO<sub>2</sub> interactions. *Geochemical transactions*, 12(1), 9.
- (20) Fu, Q., Lu, P., Konishi, H., Dilmore, R., Xu, H., Seyfried, W. E., & Zhu, C. (2009). Coupled alkali-feldspar dissolution and secondary mineral precipitation in batch systems: 1. New experiments at 200 °C and 300 bars. *Chemical Geology*, 258(3), 125-135.
- (21) Yu, Z., Liu, L., Yang, S., Li, S. and Yang, Y. (2012). An Experimental Study of CO<sub>2</sub>-brine-rock Interaction at in Situ Pressure-temperature Reservoir Conditions. *Chemical Geology*. 326–327: 88–101.
- (22) Craft, B. C., Hawkins, M. F., Terry, R. E. Applied Petroleum Reservoir Engineering (2nd Edition). Prentice Hall, Englewood Cliffs, NJ, p 431, **1991**. ISBN: 0130398845.
- (23) Brunet, J. P. L.; Li, L.; Karpyn, Z. T.; Kutchko, B. G.; Strazisar, B. and Bromhal, G. Dynamic evolution of cement composition and transport properties under conditions relevant to geological carbon sequestration. *Energ. Fuel*, **2013**, 27(8), 4208-4220. DOI: 10.1021/ef302023v.
- (24) Rimmelé, G., Barlet-Gouédard, V., & Renard, F. (2010). Evolution of the petrophysical and mineralogical properties of two reservoir rocks under thermodynamic conditions relevant for CO<sub>2</sub> geological storage at 3 km depth. Oil & Gas Science and Technology–Revue de l'Institut Français du Pétrole, 65(4), 565-580.

**Table 1:** Mineral composition of unreacted Knox sandstone and minerals produced as a result of the interaction between sandstone and CO<sub>2</sub>-saturated brine. The compositions of unreacted Knox sandstone are assigned based on information in Carroll et al. (2012) and Soong et al. (2014). Please refer to Zhang et al. (2015) for details of how specific surface areas and molar volumes of minerals are determined.

Mineral name	Volume percentage (%, before reaction with brine and CO <sub>2</sub> )	Specific surface area (m²/g)	Molar volume (cm³/mol)		
Mineral compositions of unreacted Knox sandstone					
Annite $(KFe_3AlSi_3O_{10}(OH)_2)$	0.14	7.43	154.3		
Ba-rich feldspar	0.02	0.39	100.4		
$(BaAl_2Si_2O_8)$					
Microcline (KAlSi <sub>3</sub> O <sub>8</sub> )	7.90	0.39	100.4		
Muscovite/Illite	4.00	3.40	144.5		
$(K_{0.85}Al_{2.85}Si_{3.15}O_{10}(OH)_2)$					
Na-rich feldspar	14.1	0.39	100.4		
$(NaAlSi_3O_8)$					
Quartz (SiO <sub>2</sub> )	69.8	0.10	22.7		
Trace mineral <sup>a</sup>	2.64	0.0005	22.7		
Porosity	1.40				
Minerals produced as a result	of sandstone—CO <sub>2</sub> -sa	turated brine in	teraction		
Barite (BaSO <sub>4</sub> )	0	1.85	52.1		
Calcite (CaCO <sub>3</sub> )	0	1.00	36.9		
Dolomite $(CaMg(CO_3)_2)$	0	0.10	64.3		
Gypsum $(CaSO_4 \cdot 2H_2O)$	0	7.50	74.7		
Kaolinite $(Al_2Si_2O_5(OH)_4)$	0	15.0	99.3		
Montmorillinite <sup>b</sup> $(Ca_{0.165}Mg_{0.33}Al_{1.67}Si_4O_{10}(OH)_2)$	0	1.09	155.8		
SiO <sub>2</sub> (am)	0	1.62	22.7		
Siderite (FeCO <sub>3</sub> )	0	9.8×10 <sup>-4 c</sup>	29.4		

# Note

a: Here we assume that the trace minerals do not react with  $CO_2$ -saturated brine, and thus the trace minerals are assigned a very low dissolution/precipitation rate constant ( $k=10^{-20}$  mol/m<sup>2</sup>/s). Therefore, the dissolution/precipitation of the trace minerals can be ignored.

b: Specific surface area of montmorillinite is taken from Carroll et al. (2012), and molar volume of montmorillinite is calculated based on montmorillinite density data (2.35 g/cm<sup>3</sup>) in Barthelmy (2014).

c: This surface area is taken from Xu et al. (2005). This surface area is small compared with other surface area values in Table 1 because a relatively large reaction rate constant ( $k_{25}$ ) of  $1.26\times10^{-9}$  mol/( $m^2s$ ) is associated with this small surface area in Xu et al. (2005). This paper uses the same  $k_{25}$  as that used in Xu et al. (2005).

**Table 2:** Initial brine composition in Soong et al. (2014) and initial brine composition used in CrunchFlow.

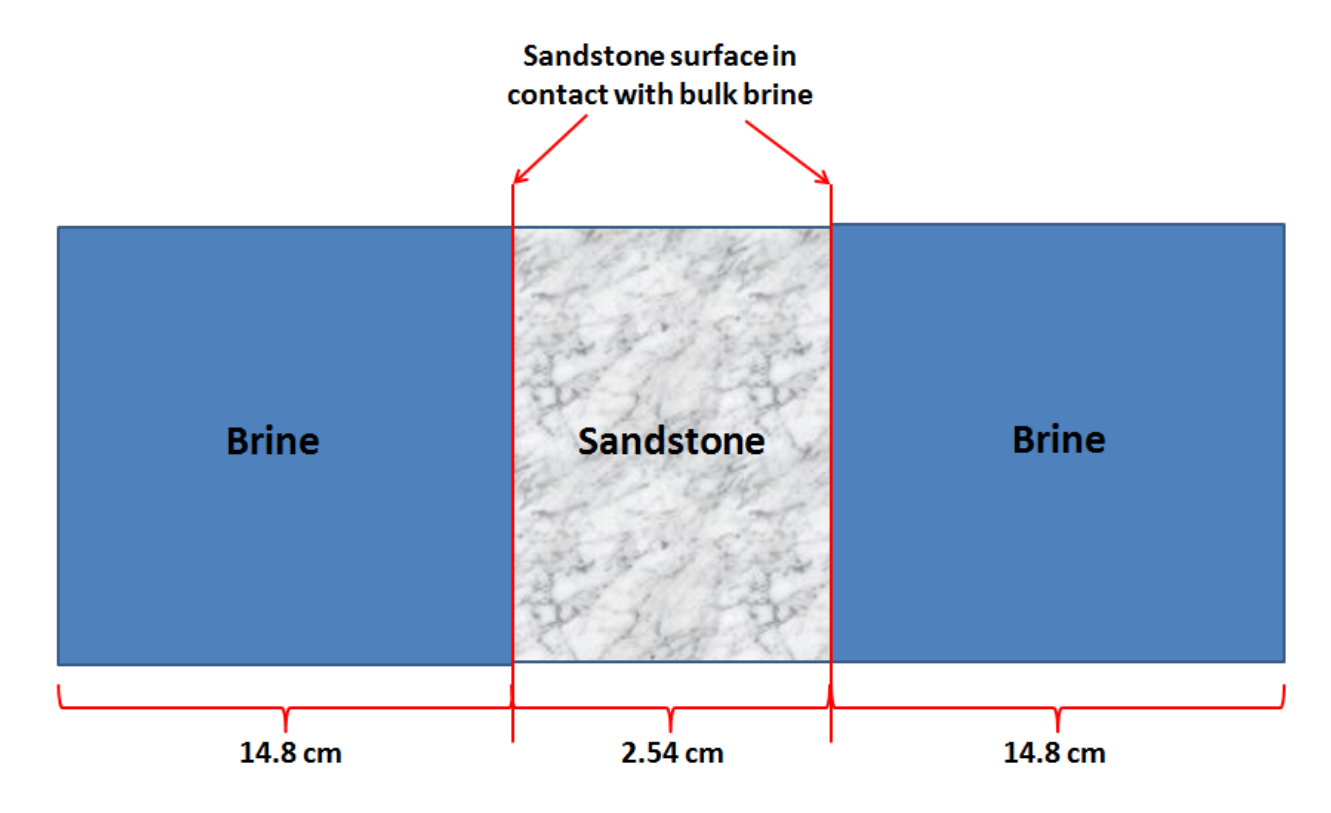
Brine composition in Soong et al. (2014) (measured at 25 °C; before	Brine composition used in CrunchFlow (calculated at 85 °C; after
injection of CO <sub>2</sub> )	injection of CO <sub>2</sub> )
Unit: mol/kg	Unit: mol/kg
pH = 5.40	pH = 4.13
$[H^+] = 3.59 \times 10^{-6}$	$[H^+] = 7.41 \times 10^{-5}$
$[Ca^{2+}] = 0.47$	$[Ca^{2+}] = 0.47$
$[Na^+] = 1.48$	$[Na^{+}] = 1.48$
$[Mg^{2+}] = 0.099$	$[Mg^{2+}] = 0.099$
$[K^{+}] = 0.036$	$[K^{+}] = 0.036$
$[Ba^{2+}] = 5.71 \times 10^{-5}$	$[Ba^{2+}] = 9.64 \times 10^{-7}$
$[SO_4^{2-}] = 4.84 \times 10^{-3}$	$[SO_4^{2-}] = 4.78 \times 10^{-3}$
$[H_4SiO_4] = 1.61 \times 10^{-5}$	$[H_4SiO_4] = 6.24 \times 10^{-6}$
$[C1^-] = 2.97$	$[C1^{-}] = 2.97$
$[Al^{3+}] = 1.00 \times 10^{-5}$	$[Al^{3+}] = 1.15 \times 10^{-7}$
$[Fe^{2+}] = 1.42 \times 10^{-3}$	$[Fe^{2+}] = 1.42 \times 10^{-3}$
$[CO_2]_{tot} = N/A$	$[CO_2]_{tot} = 0.689$

Note: All concentrations are total concentrations that take account of speciation. CrunchFlow predicts that the brine is super-saturated with  $BaSO_4$  and muscovite at 85  $^{\circ}C$ , and CrunchFlow uses  $[Al^{3+}]$ ,  $[Ba^{2+}]$  and  $[H_4SiO_4]$  concentrations after the super-saturation is accounted. All values reported in Table 2 are in the unit of mol/kg. A brine density of  $1.11 \times 10^3$  kg/m³ was used to convert mg/L values in Soong et al. (2014) into mol/kg. The brine density was calculated based on a brine density calculator (Computer Support Group, Inc., 2014).

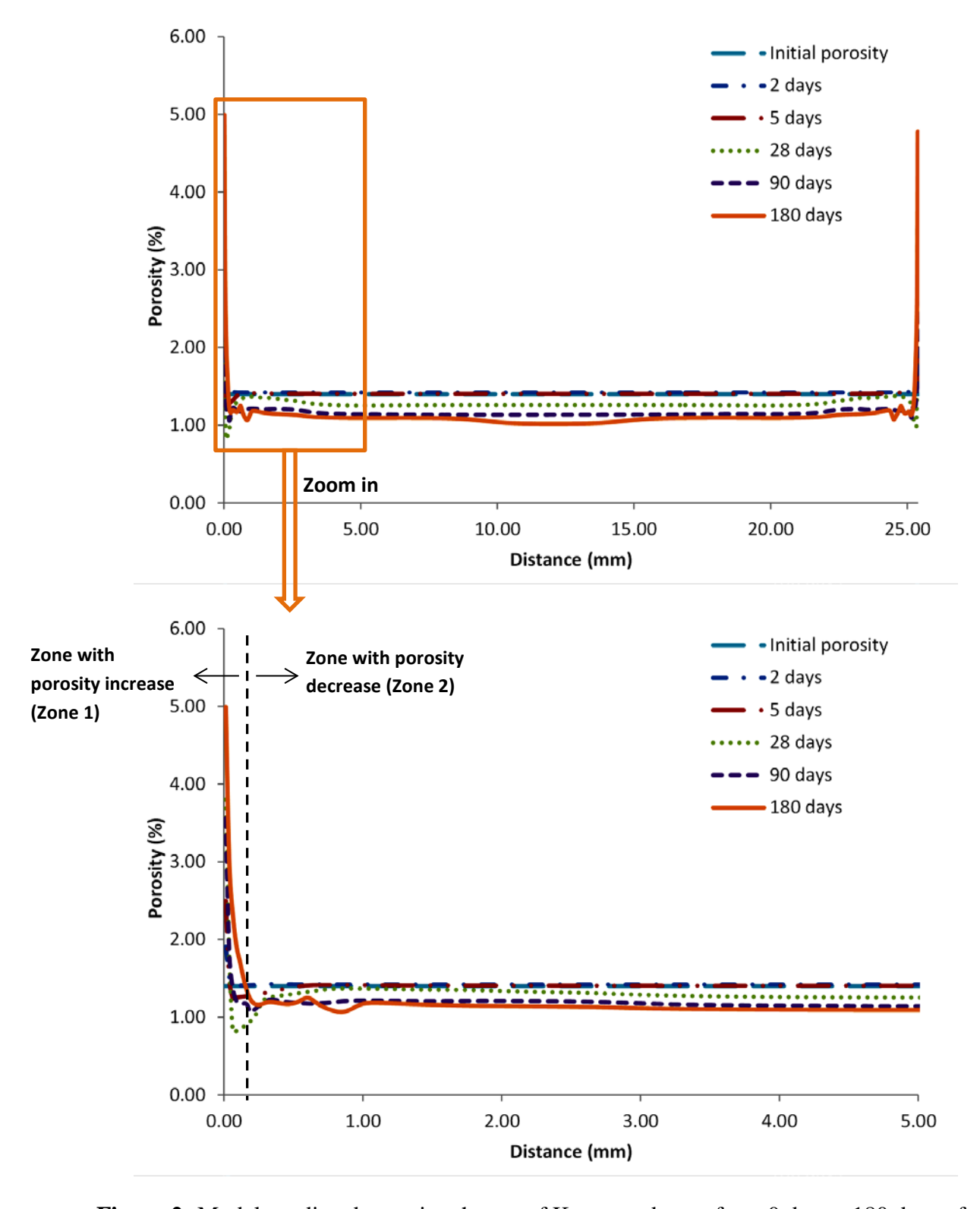
**Table 3:** Comparison between model-predicted major element concentrations and laboratory-measured major element concentrations in brine after 180 days of exposure.

Element	Measured concentration (mg/kg water)	Model- predicted concentration (mg/kg water)
Ca	19,479	18,797
Na	34,915	33,972
Mg	2,427	2,376
K	1,472	1,449
Fe	91.9	145
Si	10.0	17.8
Al	1.42	0.26
Ba	2.95	0.13
С	Not measured	8,268

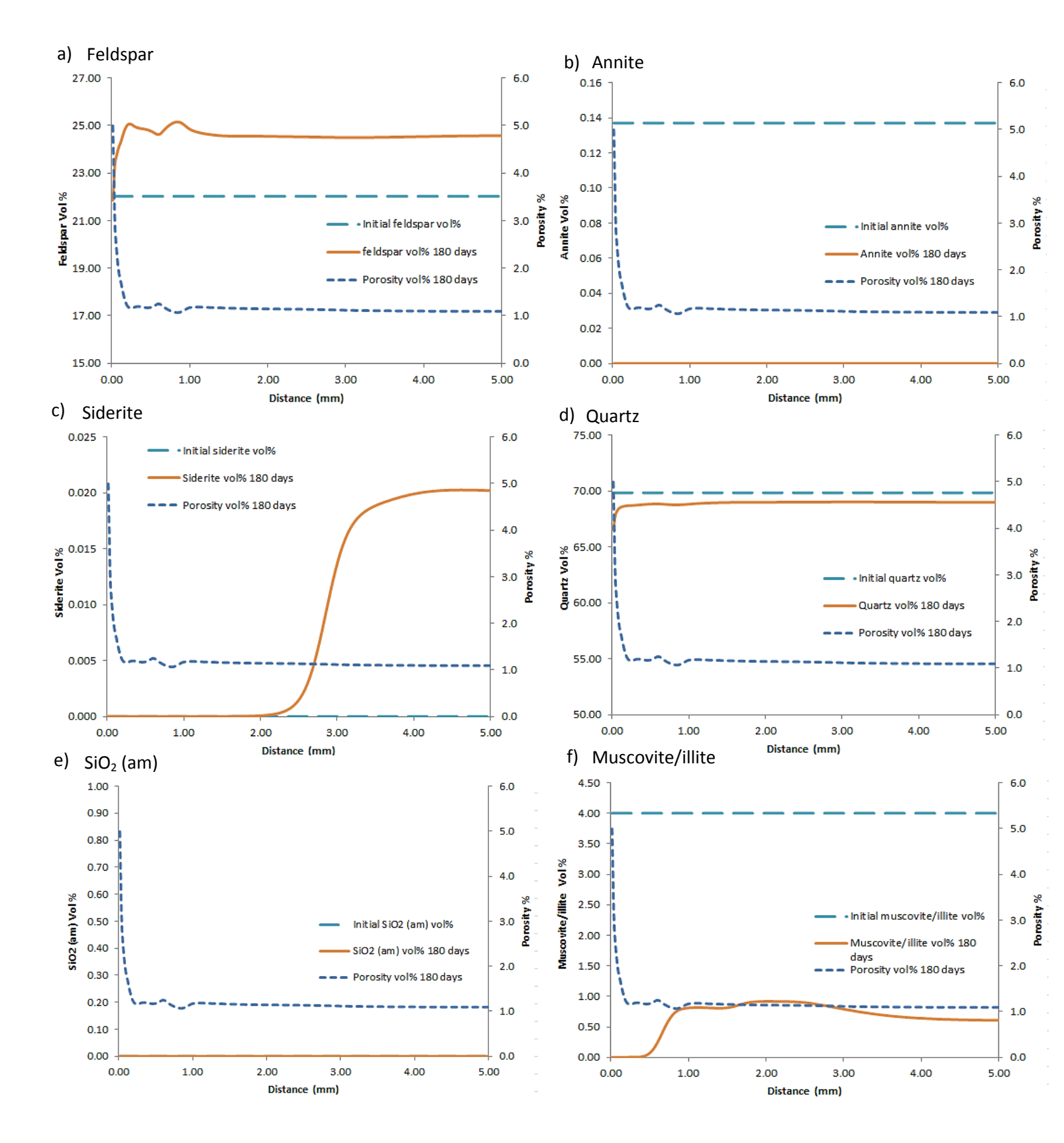
Note: The measured concentration values in this table are the average of 3 individual measurements (Soong et al., 2014). When the element concentrations were measured in Soong et al. (2014), the brine was acidified and pH was dropped to 2.0. Therefore, brine pH after exposure needs to be reduced to 2.0 in CrunchFlow to make CrunchFlow results comparable to measurements in Soong et al. (2014).

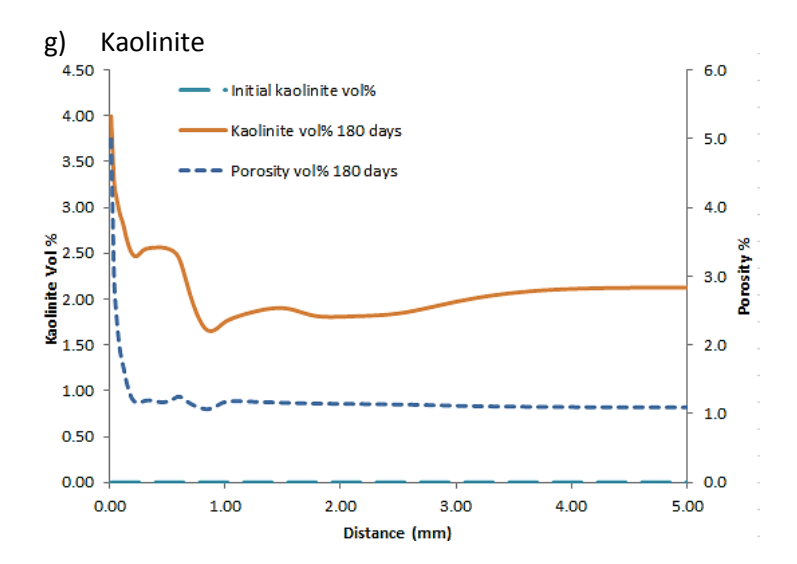


**Figure 1:** Schematic of the modeling region used in simulating sandstone core chemical alteration, and predicting associated permeability changes (not to scale).

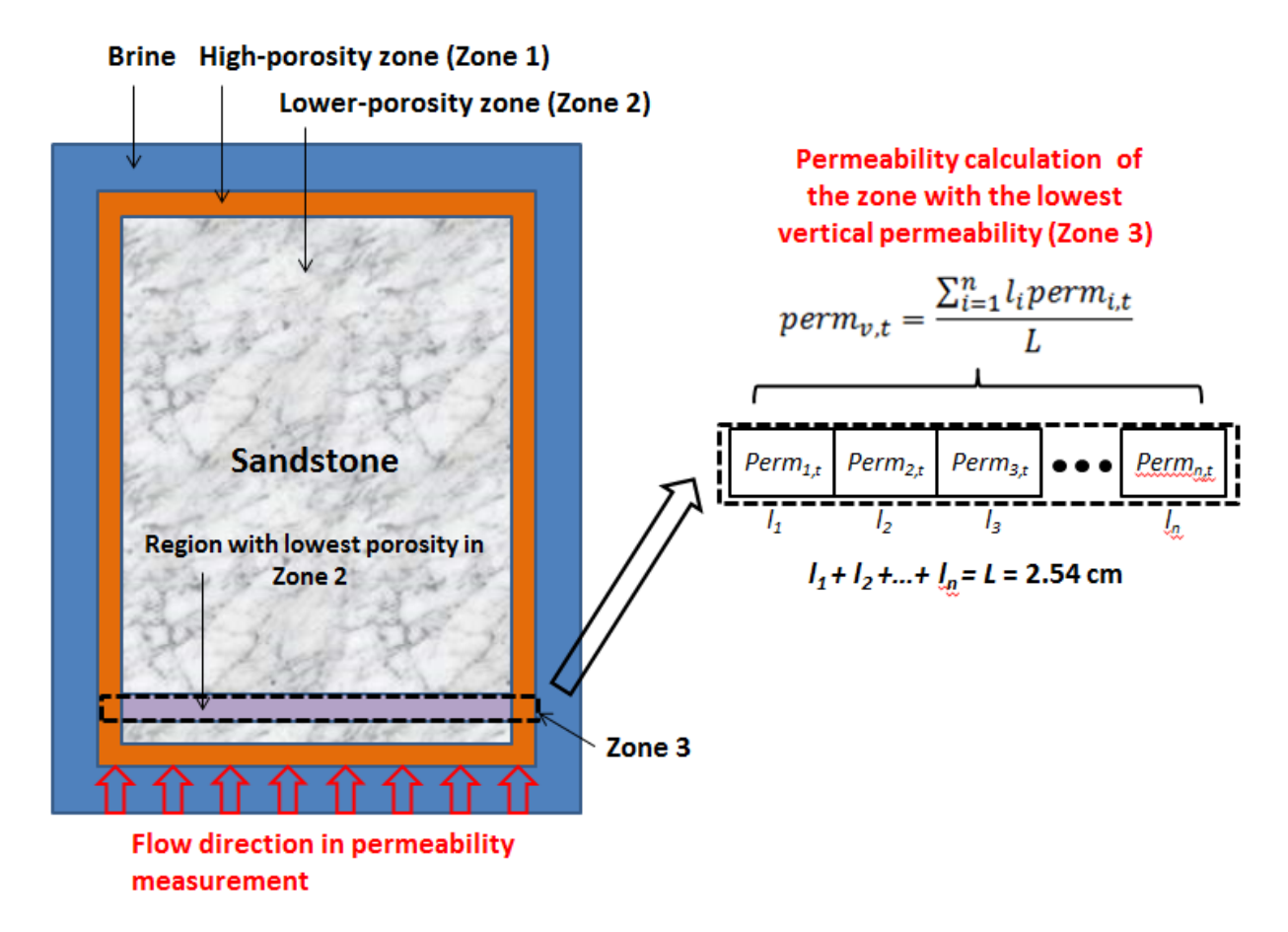


**Figure 2:** Model-predicted porosity change of Knox sandstone from 0 day to 180 days of exposure to CO<sub>2</sub>-saturated brine. The distance in Figure 2 refers to the distance away from the sandstone surface.

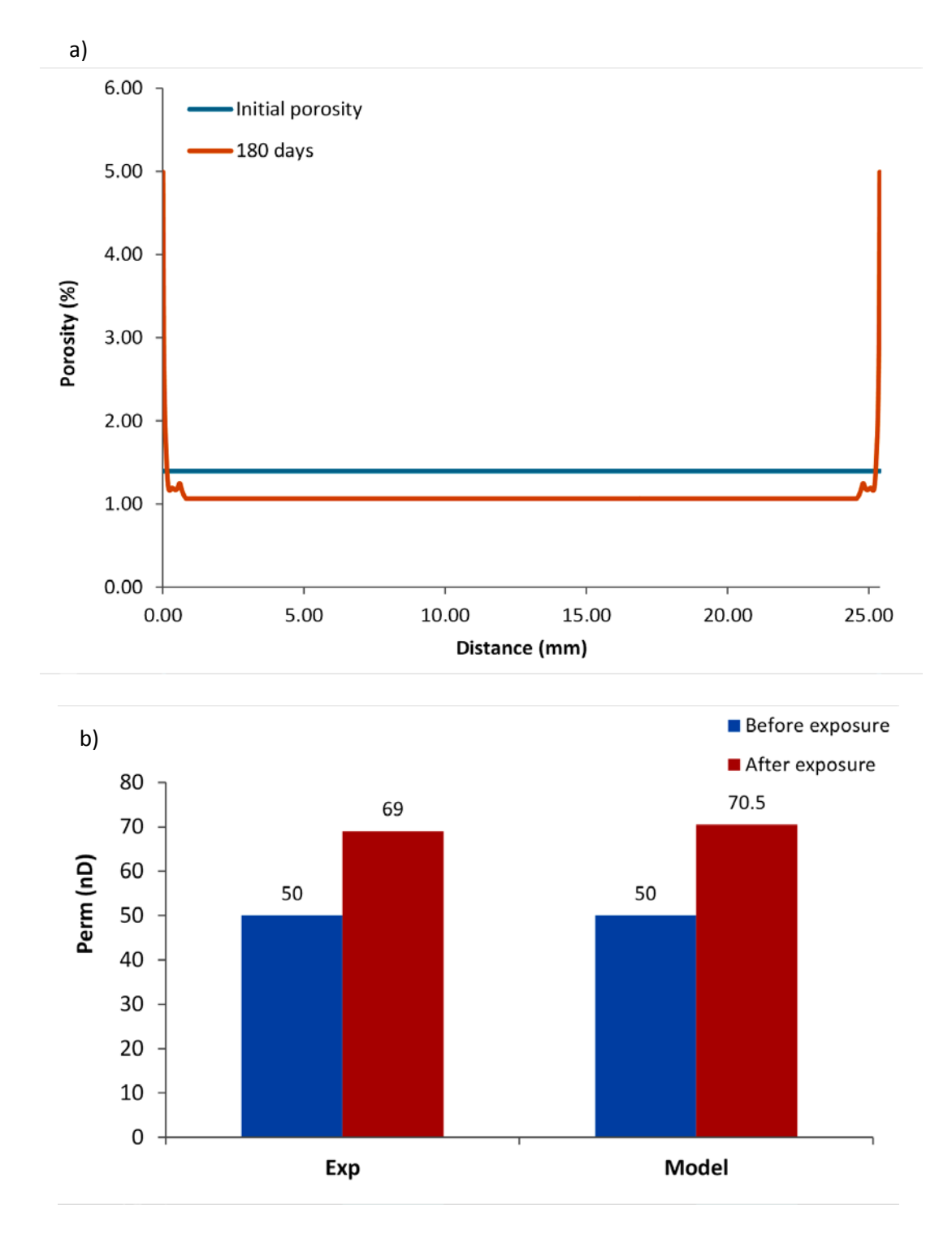




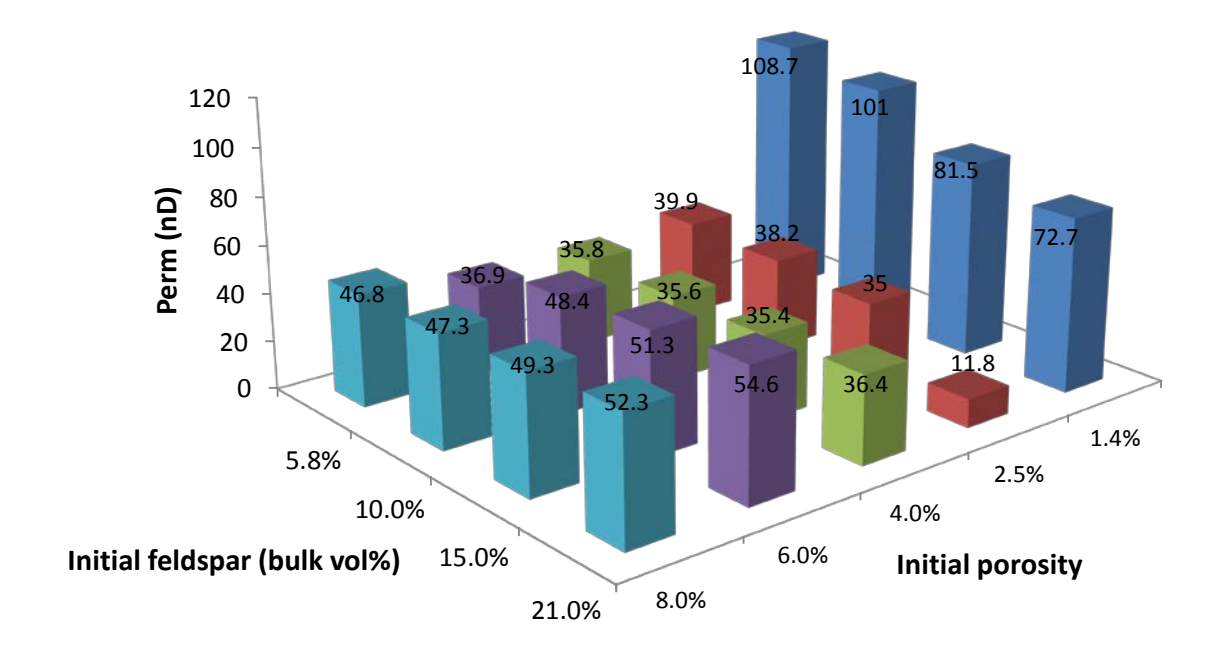
**Figure 3:** Model-predicted mineral vol% change of Knox sandstone after 180 days of exposure to CO<sub>2</sub>-saturated brine. a) Feldspar vol% change; b) Annite vol% change; c) Siderite vol% change; d) Quartz vol% change; e) SiO<sub>2</sub> (am) vol% change; f) Muscovite/illite vol% change; g) Kaolinite vol% change. The distance in Figure 3 refers to the distance away from the surface of the sandstone.



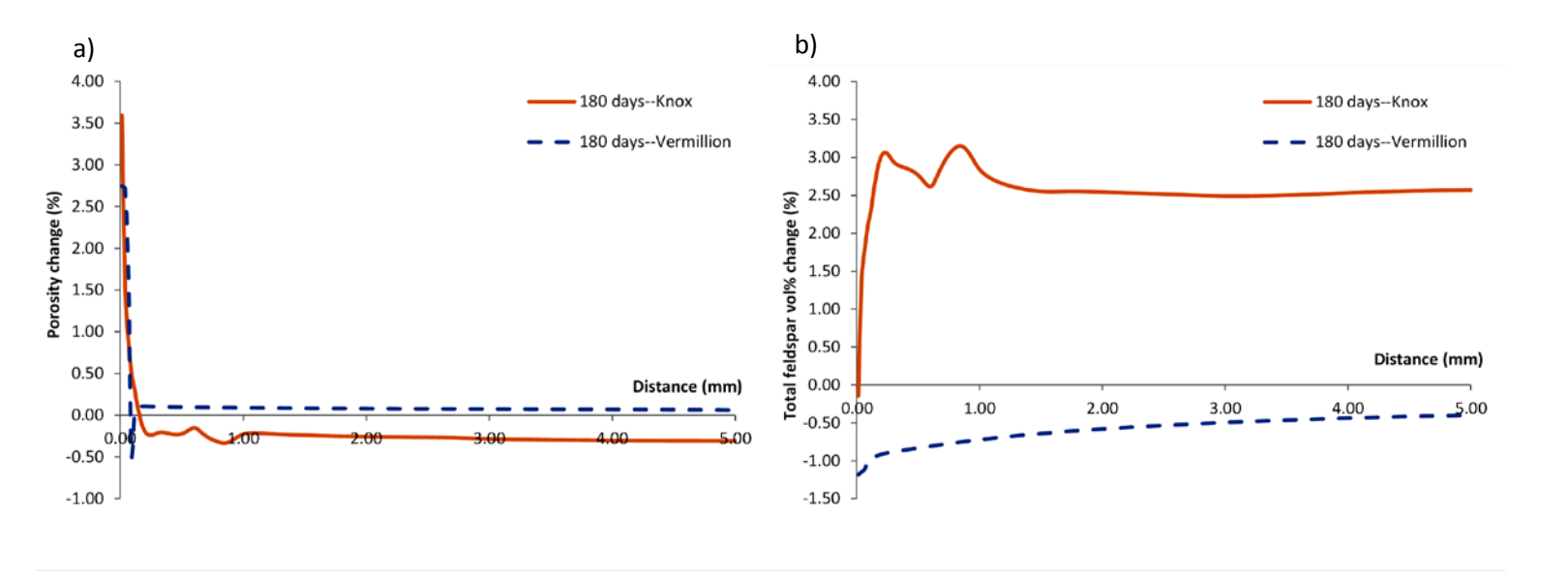
**Figure 4:** Demonstration of permeability calculation. The permeability of the zone with the lowest vertical permeability (Zone 3) is approximately the same as the vertical permeability of the entire sample. Please note that Zone 3 is composed of several grid blocks that have high permeability at edges (those grid blocks are at Zone 1), and other grid blocks that have low permeability in the middle (those grid blocks are at Zone 2).



**Figure 5:** Porosity distribution in Zone 3 (a), and the permeability of Zone 3 calculated from porosity distribution (b).



**Figure 6:** Sensitivity analysis results showing the impact of initial porosity and initial feldspar content change on permeability change after 180 days of exposure. The permeability before exposure is 50 nD.



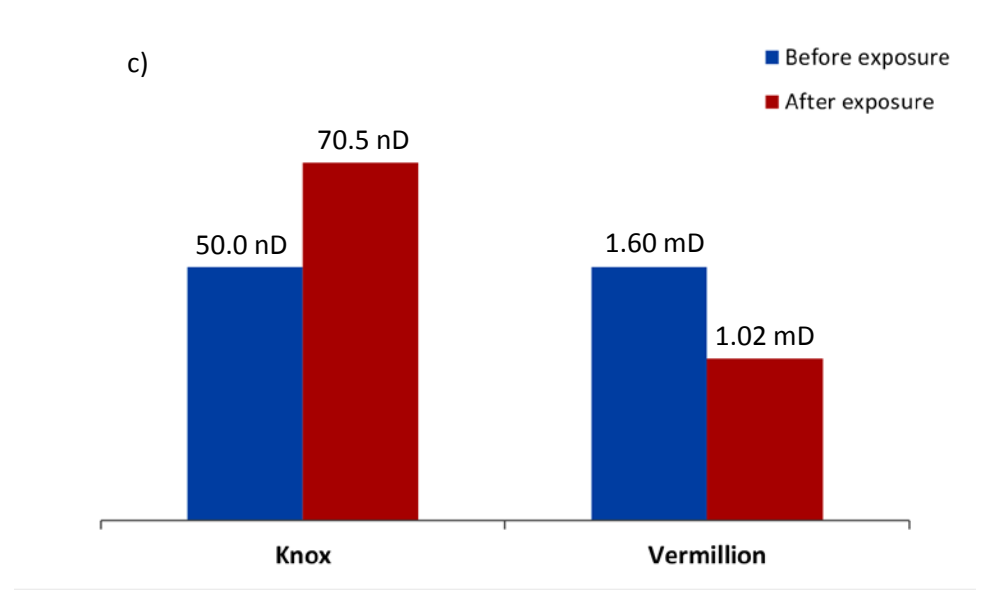


**Figure 7:** a) Porosity change of the Knox sample *v.s.* porosity change of the Vermillion sample after 180 days of exposure. Porosity change = porosity after 180 days of exposure — porosity of unreacted sample; b) total feldspar vol% change of the Knox sample *v.s.* total feldspar vol% change of the Vermillion sample after 180 days of exposure. Total feldspar vol% change = total feldspar vol% after 180 days of exposure — total feldspar vol% of unreacted sample; c) permeability change of the Knox sample vs. permeability change of the Vermillion sample after 180 days of exposure.

## **Supporting Information**

Liwei Zhang, Yee Soong and Robert Dilmore

#### 1. Key assumptions of CrunchFlow

- 1) Fluid density does not change with pressure, i.e., fluid is non-condensable fluid.
- 2) Heat absorption and release of chemical reactions are ignored, i.e., chemical reactions do not change temperature of the system.
- 3) Attachment and detachment of ions from mineral surfaces is the rate-limiting step (i.e., a surface reaction-controlled rate law).
- 4) Mineral precipitation and dissolution do not have mechanical impact on porosity.

### 2. Important governing equations used in the model

Mass conservation equation

<u>The model used in this study is a no flow 1-D model.</u> The expression of <u>1-D</u> mass conservation equation for aqueous species i in no-flow condition is given by (Steefel and Lasaga, 1994; Zhang et al., 2013):

$$\frac{d(\phi C_i)}{dt} = \frac{d}{dx}(\phi D_{ie} \frac{dC_i}{dx}) \pm \sum_{i=1}^{N} v_{ir} R_{ir}$$

Diffusion term Reaction term

where  $\phi$  is porosity,  $C_i$  is the concentration of species i (mol/m³),  $D_{ie}$  is the effective diffusion coefficient of species i (m²/s), u is flow velocity (m/s),  $R_{ir}$  is the rth reaction rate that can produce or consume species i (mol/m³·s) and  $v_{ir}$  is stoichiometric number of species i in the rth reaction (unitless).

Mineral dissolution/precipitation rate equation

The mineral dissolution/precipitation rate equation is given by (Steefel, 2009; Zhang et al., 2013):

$$R_{ir} = A(\sum_{l=1}^{M} k_l (\prod_{i=1}^{N} a_i^{p_i}) \left(1 - \frac{Q}{K_{eq}}\right)$$

where A is the surface area ( $m^2/m^3$  porous media) of the mineral involved in the reaction,  $k_l$  is the lth parallel reaction rate ( $mol/m^2 \cdot s$ ) that contributes to the dissolution/precipitation of the mineral,  $\prod_{i=1}^N a_i^{p_i}$  describes the effects of various ions in solution on the dissolution/precipitation rate of parallel reaction l (corresponding to  $k_l$ ), Q is the reaction quotient, and  $K_{eq}$  is the reaction equilibrium constant. The reaction quotient (Q) is equal to the product of concentrations of aqueous species in the product side of the reaction divided by the product of concentrations of aqueous species in the reactant side of the reaction.

### Porosity equation

The porosity of the sandstone can be expressed as a function of the volume fractions of all mineral phases (Steefel, 2009; Zhang et al., 2013):

$$\phi(t) = 1 - \sum_{i=1}^{m} fr_i(t) - fr_n$$

where  $\phi(t)$  is the porosity at time t;  $\operatorname{fr_i}(t)$  is the volume fraction of reactive mineral phase i at time t, and  $\operatorname{fr_i}(t)$  is calculated by the mineral dissolution/precipitation reaction;  $\operatorname{fr_n}$  is the volume fraction of all inert mineral phases.

#### 3. Initial and boundary conditions used in the model[121]

In order to run a reactive transport or a reaction path calculation in CrunchFlow, initial conditions must be set. Crunchflow requires following initial conditions to be specified: 1) mineral compositions (vol%) of each domain; 2) porosity of each domain; 3) total concentrations of all aqueous species in each domain. Our model has two domains: brine domain and sandstone domain. For brine domain, all mineral compositions are set as 10<sup>-8</sup> vol%, porosity is set as 100%, and total concentrations of aqueous species can be found in Table S-1. For sandstone domain, initial mineral compositions can be found in Table 1, porosity is 1.40%, and total concentrations of aqueous species in sandstone pore spaces are the same as those in brine domain.

**Table S-1:** <u>Total concentrations of aqueous species</u> in brine (initial condition)

Aqueous species	Concentration (mol/kg)
$[H^{+}]$	7.41E-5
$[Ca^{2+}]$	0.47
$[Na^+]$	1.80
$[Mg^{2+}]$	0.099
$[K^+]$	0.036
$[Ba^{2+}]$	9.64E-7
[SO <sub>4</sub> <sup>2-</sup> ]	4.78E-3
[H <sub>4</sub> SiO <sub>4</sub> ]	6.24E-6
[Cl <sup>-</sup> ]	2.97
[Al <sup>3+</sup> ]	1.15E-7
$[Fe^{2+}]$	1.42E-3
$[CO_2]$	0.689

This model applies no-flux condition as the boundary condition. In this case, both the advective flux and the dispersive/diffusive fluxes at the boundaries are equal to zero, which mimics the no-flow exposure experiment in Soong et al. (2014). Pressure and temperature at boundaries are fixed and do not change with time.

# 4. Justification of using n = 4.9 in Eqn. 2

**Table S-2:** Model-predicted permeability values given different n values (n = 11, 5, 4.9 and 4.5) in Eqn. 2. The model-predicted permeability (70.4 nD given an n value of 4.9) is very close to laboratory-measured permeability (69 nD).

Exponent n value	perm (nD)
n=11	1.19×10 <sup>5</sup>
<i>n</i> =5	77.3
n=4.9	70.4
n=4.5	50.3
Measured perm	69

## References

Lichtner, P.C., 1992. Time–space continuum description of fluid/rock interaction in permeable media. J. Geophys. Res., 3135-3155.

Steefel, C. I., & Lasaga, A. C., 1994. A coupled model for transport of multiple chemical-species and kinetic precipitation dissolution reactions with application to reactive flow in single-phase hydrothermal systems. American Journal of Science, (294), 529-592.

Steefel, C. I., 2009. CrunchFlow User's Manual. Lawrence Berkeley National Laboratory, Berkeley, CA.

Strang, G., 1968. On the construction and comparison of difference schemes, SIAM J. Numer. Anal., 506-517.

Zhang, L., Dzombak, D. A., Nakles, D. V., Brunet, J. P. L. and Li, L., 2013. Reactive Transport Modeling of Interactions between Acid Gas (CO<sub>2</sub> + H<sub>2</sub>S) and Pozzolan-Amended Wellbore Cement under Geologic Carbon Sequestration Conditions. Energy & Fuel, 27(11), 6921-6937.

Zysset, A., Stauffer, F. and Dracos, T., 1994. Modeling of chemically reactive groundwater transport, Water Resources Res., 2217-2228.